Precision measurement of the Sherman asymmetry function for electron scattering from gold

A. Gellrich and J. Kessler
Physikalisches Institut der Universität Münster, D-4400 Münster, Germany
(Received 16 March 1990)

Measurements of the asymmetry (Sherman) function for gold as a function of foil thickness have been made in a "classical" electron double-scattering experiment. Results are presented for incident energies of 50 and 120 keV at scattering angles of 45°, 60°, 75°, 105°, 110°, 115°, 120°, 125°, and 130°. The measurements were highly reproducible owing to the consistent method we used for coping with spurious asymmetries. Absolute values of the asymmetry function were determined using two identical foils of 222 $\mu g/cm^2$ at 120 keV and 71 $\mu g/cm^2$ at 50 keV. An analysis of the uncertainties at these calibration points shows that they are below 0.3%. Extrapolation of the data to zero foil thickness and comparison with theory are critically discussed.

I. INTRODUCTION

The discussion of the accuracy of electron polarimetry by Mott scattering has revived in the past few years. This issue came up because of major advances in polarized-electron sources, which had the consequence that the accuracy of many experiments with polarized electrons is no longer limited by statistics but rather by the uncertainty in the measurement of electron polarization.

Although some new ideas on electron-polarization analysis that have been realized in the past few years have their merits in special cases (for a survey see Ref. 1), the majority of polarization analyzers still exploits the old principle of the Mott detector: if an electron beam which is scattered by a target of high atomic number Z has a polarization P normal to the scattering plane, one obtains a left-right asymmetry

$$A=(L-R)/(L+R) \tag{1}$$

of the scattered intensities (L and R are the intensities scattered through the same angle θ to the left and right, respectively). From this asymmetry one can determine the polarization

$$P=A/S_{\text{eff}} \tag{2}$$

if the analyzing power S_{eff} (asymmetry function, Sherman function) of the target is known. The subscript denotes that in a real experiment one has to use the effective analyzing power of the target rather than the analyzing power of a single atom, which is usually calculated theoretically.

It is a drawback of the Mott detector that the conventional methods of determining S_{eff} are not very accurate. Its exact value is affected by multiple and plural scattering and depends in a complicated way on the design parameters of the analyzer, such as thickness of the target, energy discrimination of the scattered electrons, and solid angle subtended by the detectors. Theoretical treatments of the influence of multiple and plural scattering on S_{eff} are not very accurate, and the overall uncertainty of S_{eff} attained by the method of extrapolation to zero thickness of the target foil where the theoretical free-atom value S should hold is not smaller than ±5%. This has been shown by a careful experimental analysis by Fletcher *et al.*,[2] which is an invaluable counterbalance to many overly optimistic but less realistic papers claiming error limits for their absolute polarization measurements down to 1%.

The most straightforward and conceptually simplest method of determining the Sherman function is double scattering. It takes advantage of the well-established equality of the polarizing and analyzing power in elastic scattering. As indicated in Fig. 1, the first scattering process produces a polarization P which is given by the effective Sherman function S_{eff} of the first scattering process: $P=S_{\text{eff}}$. If the parameters of the second scattering process (electron energy, angles, target) are the same, the left-right asymmetry A is governed by the same value of the Sherman function S_{eff},

$$A=PS_{\text{eff}}=S_{\text{eff}}^2 , \tag{3}$$

where $P=S_{\text{eff}}$ has been taken into account.

Such absolute measurements of the Sherman function by double scattering have been done several decades ago by various groups (for a review of earlier work see Ref. 3), the most elaborate work being that of van Klinken.[4]

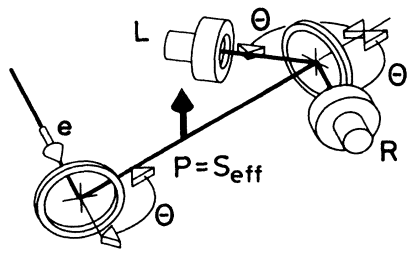

FIG. 1. Double-scattering experiment. L and R denote the detected intensities in the left and right counter, P and S_{eff} are explained in Eq. (2).

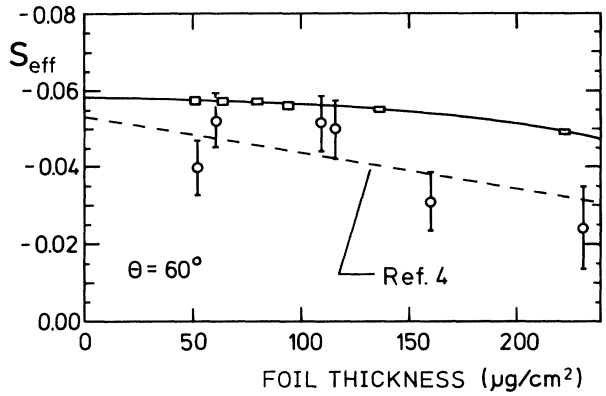

FIG. 2. Effective Sherman function of gold. Results of the present experiment (120 keV, rectangles; their size indicates the experimental uncertainty) and van Klinken's experiment Ref. 4 (121 keV, circles) at 60°.

Unfortunately, the uncertainties of the early measurements are fairly large, so that the accuracy of recent polarization experiments is usually limited by the uncertainty of the Sherman function of the Mott detector used for polarization analysis. As an example, Fig. 2 shows a result of the classic van Klinken experiment at 121 keV, an energy typical of many Mott detectors. It is obvious that the scatter of the experimental data prevents a determination of the analyzing power with an accuracy in the 1% region. Only if such an accuracy could be achieved, the polarization analysis would no longer be the weakest point in a polarization experiment.

It is the object of the present paper to obtain experimental results of the Sherman function with good reproducibility and high accuracy. The example given in Fig. 2 shows that this goal has been reached.

II. EXPERIMENTAL PROCEDURE

Although an experiment aiming at a considerable improvement of the accuracy cannot just be a repetition of earlier work, the principle used here is the conventional double-scattering experiment given in Fig. 1. In a first step, the effective Sherman function is determined according to Eq. (3) for a well-defined set of scattering parameters. Let us denote it by S'_{eff}. Second, the dependence of the effective Sherman function on the scattering parameters, in particular θ and foil thickness t, is observed. This is done by varying θ and t in scattering process number 1, while leaving scattering process number 2 unchanged. Accordingly, scattering 1 yields the polarization $P = S_{\text{eff}}(\theta,t)$ and scattering 2 yields the asymmetry

$$A = PS'_{\text{eff}} = S_{\text{eff}}(\theta,t)S'_{\text{eff}} \ . \tag{4}$$

From the measured values of A in conjunction with the values of S'_{eff} found in the first step of the experiment one obtains $S_{\text{eff}}(\theta,t)$.

We will now briefly indicate why in the present experiment a considerable improvement of accuracy was achieved. The main reason is the consistent method we used for coping with instrumental, i.e., spurious asymmetries. Since the method is described in detail elsewhere,[5] we will give here only the basic facts without proving them.

While certain types of instrumental asymmetries can easily be eliminated, there are other types which are more difficult to cope with (cf. Ref. 1, Chap. 8.1.2). An example for the latter type is the asymmetry resulting from a misalignment of the polarized electron beam entering the Mott detector in an experiment, where the electron polarization cannot be easily reversed. One has this situation in a double-scattering experiment, where the polarization of the electrons emerging from the first target can only be reversed by changing the geometry of the arrangement. This makes the elimination of instrumental asymmetries more difficult than in an experiment with polarized electrons from a GaAs source, where the electron polarization can easily be reversed by reversal of the circular polarization of the light used for photoemission. In order to cope with such false asymmetries one can, in addition to the polarization counters of the Mott detector, introduce a pair of monitor counters at small scattering angles where due to the vanishing Sherman function (cf. Fig. 3) no genuine scattering asymmetry will occur. If these monitor counters register an asymmetry, it must be instrumental. If they do not register an asymmetry, one must, however, not conclude that one has ideal axial incidence of the polarized electrons. This is because the instrumental asymmetries caused by the lateral displacement of the incident beam and its angle of inclination with respect to the symmetry axis of the detector system may compensate each other. Mathematically, there is an infinite number of such possibilities.

This may have been the reason why the use of monitor counters, which were more popular in the past[4,7–10] than at present,[11] often did not really improve the results and sometimes made them even more questionable. But there is another important point which was frequently overlooked. The ratio of the distances which the monitor counters and the polarization counters have from the target foil, must have the correct value. Only if this condition is fulfilled, can one find a unique relation between the instrumental asymmetries of the two pairs of counters and can thus correct for false asymmetries. This has al-

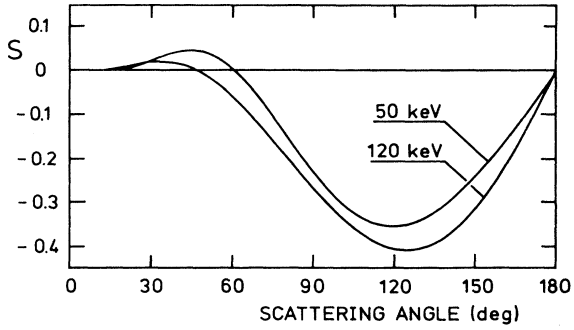

FIG. 3. Sherman function of gold at 50 and 120 keV. Theoretical values of Bühring (Ref. 6).

ready been shown by van Klinken,[4] who made, however, too simple an approximation (Rutherford distribution of the scattered electrons) for finding the correct distance of the monitor counters. If the distance is not properly chosen, any attempt of eliminating false asymmetries with the help of monitor counters leads to erroneous results.[5,12] The correct distance depends strongly on the angular dependence of the scattered intensity. That is why in the present experiment also the angular distributions of the electrons scattered from the analyzer foils have been experimentally determined. On the basis of these data, the correct distance of the counters could be determined. This procedure, albeit laborious, was worth the extra effort. The experimental asymmetries that had been corrected for false asymmetries turned out to be very reproducible and showed no appreciable scatter any more, as can clearly be seen from the results presented in the following.

The brief outline given here does not suffice to explain the details of our method of eliminating instrumental asymmetries. We emphasize that this procedure was the essential step for obtaining accurate results and refer for a more thorough presentation of this technical problem to a different record.[5]

III. APPARATUS

After leaving the accelerator tube, the incident unpolarized electron beam is focussed by a deflection coil (from a television set) onto the polarizer foil in the center of the scattering chamber (see Fig. 4). If the foil is revolved out of the beam line, the primary electrons are collected by a Faraday cup for current measurement. A collimation assembly defines the direction of the electrons that are scattered at the polarizer foil and reach the analyzer, which can be positioned at angles θ between 45° and 130°. Electrons that are scattered at the analyzer foil for a second time are detected at an angle of 120° (polarization counters) on the left and right side. From the left-right asymmetry the absolute value of the Sherman function is calculated. The pair of counters at 45° (monitor counters) which is placed at the correct distance ratio (cf. Sec. II and Ref. 5) serves for elimination of instrumental asymmetries. The whole analyzer is rotatable through 180° in the azimuth to interchange the positions of the left and right counters (positions 0 and π of the analyzer). In the following, experimental details will be discussed.

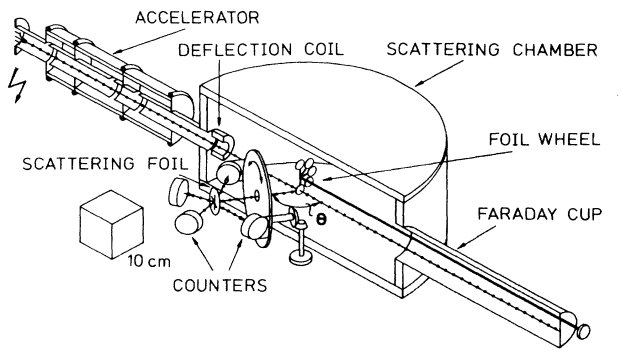

FIG. 4. Schematic view of the apparatus.

The incident beam is produced by a Steigerwald telefocus cathode followed by a three-stage electrostatic accelerator. This system yields a parallel primary beam which, without use of diaphragms, is stable in position and intensity. Scattering at diaphragm edges and extended pumping time are thus avoided.

The negative accelerating voltage (up to 120 kV) was generated by a stabilized high-voltage cascade (Glassman PG 150R3) and measured with a calibrated high-voltage resistor (200 metal-film resistor of 5 MΩ±1% in series formed a helix and were placed inside a lucite tube of 20 cm diameter and 60 cm height). The calibration was performed as follows: First, this resistor (together with the ammeter used as voltage indicator) was compared with a resistor which had been calibrated by the Physikalische Technische Bundesanstalt (national gauging office) and could be employed up to 80 kV. This results in a maximum absolute uncertainty of ±125 V below 80 kV. Second, an electron beam with now well-known energy ($\leq$80 keV) was deflected with an ironless coil by a fixed amount and the coil current (strictly proportional to the magnetic field) was measured. Via the coil current which is necessary to deflect an electron beam of another energy about the same amount, the actual high voltage was calculated relativistically and then compared with the voltage indicated by the ammeter. Such comparisons were performed at different accelerating voltages under different conditions of temperature and humidity. They showed that the high-voltage resistor works linearly up to 120 kV. The overall uncertainty of accelerating voltages between 80 and 120 kV was estimated to be within ±250 V.

We also performed an independent energy calibration with the 126.9-keV internal-conversion electrons of a ^{139}Ce source which was enclosed between titanium foils of 2.4 mg/cm^2 thickness. The titanium foils limited the final accuracy of this calibration, since the energy loss of the electrons could be determined experimentally only within ±1 keV. But within this uncertainty, agreement was obtained between the different calibration methods.

The electron gun and the associated power supplies are isolated at negative high voltage, while the scattering chamber with polarizer and analyzer is grounded. A wheel consisting of eight identical brass rings which support the foils offers the possibility to rotate either a gold foil as polarizer or a fluorescent screen for beam monitoring into the center of the scattering chamber. Another feature of the construction is the possibility of shifting the foil wheel by means of a micrometer gauge perpendicular to its own plane to a maximum distance of $\Delta f = 10$ mm. Thus every target foil can be positioned exactly into the center of the scattering chamber to adjust the polarized beam without breaking the vacuum. The gold foils were prepared by vacuum deposition on Pioloform (similar to Formvar) backings. The thickness of the gold foils was measured roughly with a piezoelectric frequency monitor during the deposition process. A more precise

thickness determination will be described in the next section.

The analyzer (see Fig. 5) is a closed cylinder (apart from the collimation assembly and the exit which served as electron absorber) which can be turned continuously from 45° to 130° if the scattering chamber is open. The uncertainty of the horizontal direction of both the primary beam (±0.2°) and the rotation axis (±0.2°) with respect to the goniometer limits (in conjunction with the uncertainty of the indicated angle) the accuracy of the first scattering angle to ±0.4°. After finishing the asymmetry measurements, we found that the 50-keV primary beam had an additional tilt. Consequently, all the angles of the first scattering process at 50 keV were one degree lower than indicated. The error that was caused by presuming identical angles in the first and second scattering process could, however, be corrected by utilizing our measured angular dependence of the Sherman function. This correction was performed, although it was smaller than the statistical uncertainty.

The analyzer contains four detectors (silicon surface-barrier counters, Tennelec PD 25-100-14-CM) and the associated charge-sensitive preamplifiers with 1 cm^3 volume (Amptek A-225). The detectors are positioned coplanar and symmetrically at angles of 120°±0.2° and 45°±0.2° with respect to the axis of incidence (rotation axis). The detectors can be shifted in order to adjust their proper distances for complete elimination of instrumental asymmetries (the proper distance ratio of monitor and polarization counters depends on the scattering energy and the thickness of the foil actually used in the analyzer, see Ref. 5). The solid angles subtended by the analyzer entrance and the counters (cf. Fig. 6) were chosen small enough to be of negligible influence on the final results. The complete analyzer is rotatable through 180° in the azimuth with a precision of ±0.1° as proved by a spirit level. The analyzer is rotated by means of an electric motor drive, which is mounted at a distance of 1 m from the scattering center in order to avoid disturbing effects due to changing magnetic fields.

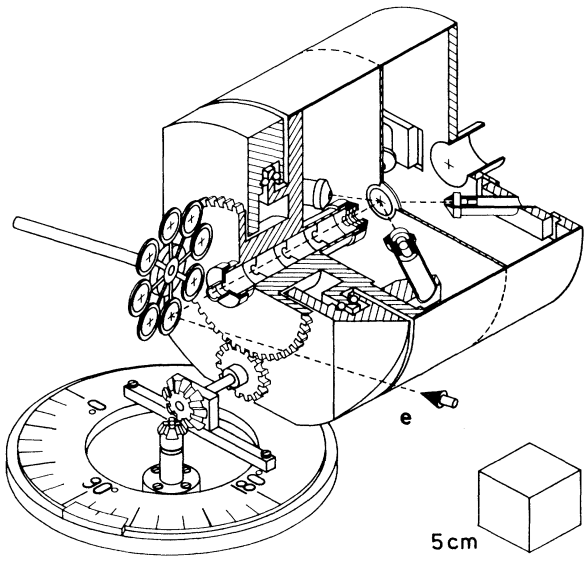

FIG. 5. Analyzer.

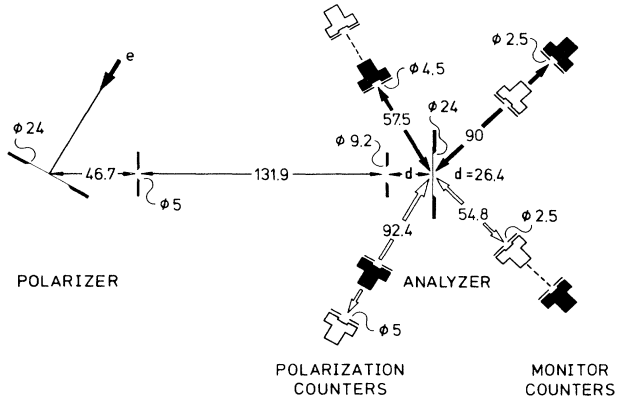

FIG. 6. Typical design parameters (in mm): black, distances h of the counters at 120 keV; white, at 50 keV. Analyzer foil 222 $\mu g/cm^2$ at 120 keV, 71 $\mu g/cm^2$ at 50 keV.

The primary beam is directed to the north, so that only the vertical component of the earth's magnetic field has to be compensated in the accelerating tube. Inside the scattering chamber this component reached a maximum value of 1 A/m. It was shown by asymmetry measurements in magnetic fields of different strengths that both static and fluctuating magnetic fields in the scattering chamber did not disturb the results. This is in principle due to the consistent method used for coping with spurious asymmetries, and made it possible to dispense with further compensation of horizontal field components. All parts of the apparatus were fabricated from nonferromagnetic materials and, where possible, were coated with graphite to reduce elastic backscattering of electrons. A turbomolecular pump maintained a vacuum of better than 1×10^{-4} Pa.

IV. EXPERIMENTAL DETAILS

A. Detector positions

It is shown in Ref. 5 that, for a reliable correction of instrumental asymmetries, the ratio $h(45°)/h(120°)$ of the distances h of monitor counters and polarization counters from the analyzer foil must have a well-defined value. This "correct" value depends strongly on the angular dependence of the scattered intensity $I(\theta)$. More precisely, it depends on the value of $E(\theta)=[1/I(\theta)]\partial I(\theta)/\partial\theta$ at the angles at which the polarization and monitor counters are positioned. In order to find the correct value of $h(45°)/h(120°)$, the angular distribution $I(\theta)$ of the electrons scattered from the analyzer foil was measured. The results (Fig. 7) deviate considerably from Rutherford distribution. This is due to the geometry of the gold foils which are of infinite extension for electrons scattered into the 90° direction. As a consequence, the intensity distribution forms a "funnel"

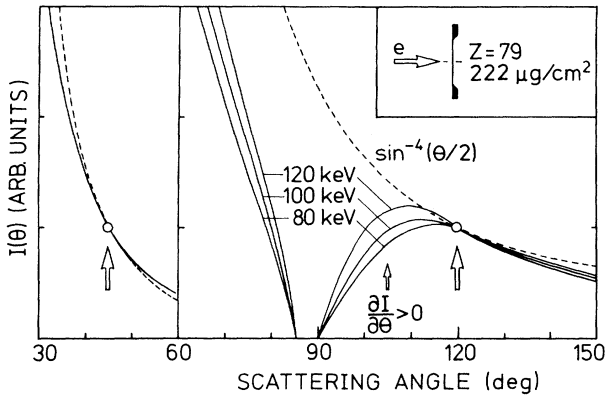

FIG. 7. Experimental intensity distributions of electrons scattered at a gold foil compared with Rutherford scattering (dashed line). The curves are fitted to one another at 45° and 120° (changed scale) to make visible the different slopes. For $\theta < 60°$ the experimental curves for these energies coincide.

around 90° which becomes broader the lower the scattering energies and the thicker the foils are.

In our analyzer we used a 222-μg/cm^2 foil at 120 keV. From the measured slope we found $E(120°) = -1.50 \pm 0.02$ rad^{-1} and $E(45°) = -4.51 \pm 0.02$ rad^{-1}. The ratio of the slopes is therefore $c = E(120°)/E(45°) = 0.333 \pm 0.006$. The significance of this value will be explained in Sec. IV D. According to Ref. 5, the measured slopes yield a correct distance ratio of $h(45°)/h(120°) = 1.56$. This is a convenient value, a result which is not necessarily warranted for other combinations of analyzer foil thickness and scattering angles. If one choses, for example, a scattering angle of $\leq 15°$ for the monitor counters (also $S \approx 0$, cf. Fig. 3) the correct distance ratio becomes smaller, so that the monitor counters have to be placed closer behind the analyzer foil. In conjunction with the small scattering angle, a separation of scattered and unscattered electrons becomes then difficult. This is why we selected an angle of 45° for the monitor counters despite the fact that $S(45°)$ is, in particular at 50 keV, not exactly zero. It will be shown in the next section that the condition $S = 0$ for the monitor counters is not as imperative as one might think.

Figure 7 shows that the maximum of the distribution of backscattered electrons ($\theta \geq 90°$) is shifted with decreasing energy to larger scattering angles. For 50 keV at 120° the slope becomes even positive while at 45° it remains negative. The consequence would be a negative distance ratio, which is impractical. We therefore chose a much thinner analyzer foil (71 μg/cm^2) for the 50-keV measurement, in order to get similar analyzer conditions as in the 120-keV measurement. With these parameters we found $E(45°) = -4.01 \pm 0.02$ rad^{-1} and $E(120°) = -0.757 \pm 0.010$ rad^{-1}. This yields a ratio $c = E(120°)/E(45°) = 0.189 \pm 0.003$ and a correct distance ratio of $h(45°)/h(120°) = 0.593$.

B. Scattering foils

Once the thickness of the two analyzer foils had been chosen, it was important for a correct calibration to produce foils of exactly the same thickness as the analyzer foils. From a set of foils for which the piezoelectric frequency monitor used during the evaporation process indicated equal thicknesses, a specimen was selected which showed at 100 keV and 130° the same scattering power (normalized scattering intensity) as the analyzer foil. Electron scattering is a sensitive method to determine differences in area densities and was therefore used to check the foils for uniformity by irradiating different parts of the same foil. This method was also applied to determine more precisely the relative foil thicknesses of all the foils as follows: Two foils (≈ 70 μg/cm^2) with equal scattering power were piled upon each other and the scattered intensity was measured. The scattering intensities versus foil thickness at 140, 70, and 0 μg/cm^2 were fitted by a second-order polynomial which then gives the relationship between the relative scattering intensity and foil thickness. According to the measurements of Lazarus and Greenberg[13] (188 keV, 110° and 120 keV, 70°) this polynomial fit can be used up to $t = 222$ μg/cm^2 (our thickest foil) and beyond. Consequently, by weighing the thickest foil where the uncertainty of the backing-foil weight is of smallest influence with a microbalance (± 2 μg), the thickness was placed on an absolute scale (see Table I). An absolute scale, though not necessary for this experiment, is useful for comparison with results in Mott scattering by other researchers. Extremely thin foils, as needed for a precise extrapolation procedure, bear some danger, a fact which was frequently overlooked: Evaporated gold tends to condense as islets[14,15] instead of forming layers of homogeneous thickness below ~ 40 μg/cm^2. Therefore, apart from the increase of the contribution of the backing, foils of (macroscopically) low area density may behave like thicker ones. To be sure to have foils of homogeneous thickness we selected a foil of 54 μg/cm^2 as the thinnest one.

TABLE I. Thicknesses of gold and backing foils. The uncertainties result from statistics, the uncertainty of weighing the 222-μg/cm^2 gold foil, the correction due to the backing foil and from the uncertainty of the extrapolation.

Applicability	Gold foil (μg/cm^2)	Backing foil (μg/cm^2)
120 keV, analyzer	222.0±2.0	10±2
120 keV	94.0±1.8	19±3
120 keV	65.7±1.5	19±3
120 and 50 keV	222.0±2.0	10±2
120 and 50 keV	135.4±1.9	10±2
120 and 50 keV	82.1±1.4	10±2
120 and 50 keV	54.0±1.3	19±3
50 keV	64.1±1.5	19±3
50 keV	71.6±1.5	19±3
50 keV	87.4±1.5	10±2
50 keV, analyzer	70.8±1.5	19±3

C. Discussion of systematic errors

The detector signals of the electrons scattered at the gold foils were monitored by a pulse-height analyzer. On the basis of the displayed electron energy-loss spectrum

shown in Fig. 8 the discriminator levels were set to optimally reject inelastic events and yet still preserve the bulk of the elastic ones. As shown by the careful analysis of Fletcher *et al.*[2] there are many events above the discriminator level which conflict with the ideal case of detecting only such electrons that have suffered single elastic scattering in both gold targets. The influence of these events on asymmetry measurements can be seen by evaluating small (but equal for all counters) areas of the spectrum, as indicated in Fig. 8. The dominant effects are inelastic scattering from the gold foil, both elastic and inelastic scattering from the backing foil, target scattering combined with wall reflection as well as multiple and plural scattering, and contributions from x-rays, noise, and the "dark-counting" rate. The influence of those effects which are exclusively caused by scattering at the gold foil is included in the definition of the "effective" Sherman function. Consequently, if the discriminator levels can be set so that all the other spurious effects are either negligible or can be easily corrected for, an evaluation of the pulse-height spectra is not necessary. In our calibration of the analyzer by double scattering at 120 keV, the discriminator levels were set near 105 keV. Needless to say, the same level was chosen at all the other measurements at 120 keV.

We shall now discuss those spurious counts which are negligible. After setting the discriminator levels we found that the "dark-counting" rate and the noise that remained when the primary electron beam was blocked was always less than 1 count/100 sec in the 50- and 120-keV measurements. A higher rate of maximum 8 counts/100 sec, but also virtually negligible, was observed for the pure x-ray contribution after covering the analyzer entrance or the detector openings by a thin aluminum foil which was inpenetrable for electrons. Then we measured and estimated the contribution of those electrons which on their way to the detectors had also suffered reflections from the walls. This was done as follows: An additional counter (with identical electronics and discriminator setting) was placed directly beside the polarizer foil and oriented along the direction to the Faraday cup. It detected the fraction of those electrons

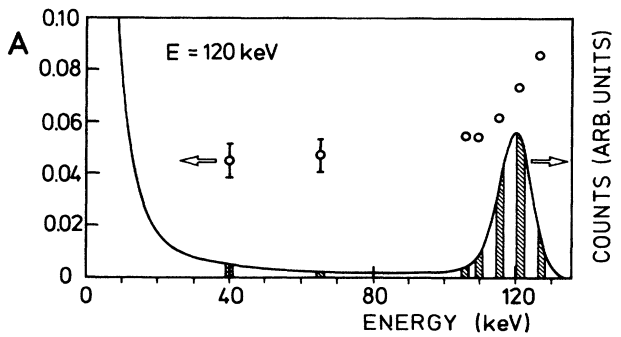

FIG. 8. Pulse-height spectrum of doubly scattered electrons. Both gold foils are 222 $\mu g/cm^2$ thick. The asymmetry values (left ordinate axis) have been measured by evaluating small (hatched) areas of the spectrum (right ordinate axis).

which, after a wall reflection, impinge upon the back of the gold foil. These electrons have to be scattered from the polarizer foil by an average angle of 50° in order to reach the analyzer which was adjusted to the (for these spurious electrons) most favorable 130° direction. Under the assumption that these electrons are unpolarized, the beam reaching the analyzer becomes depolarized by less than 0.005%. The situation inside the analyzer was much less favorable. The linear dimensions are reduced by a factor 2 or 3 compared to the scattering-chamber dimensions so that the solid angle of the electrons that reach the analyzer foil via the analyzer walls is enlarged by a factor of 4–9. Taking into account that the interior of the analyzer is also coated with graphite, this leads to an estimated reduction of the measured asymmetry by less than 0.05% (relative to the measured value). Inelastically (Møller) scattered electrons at angles $\geq 45°$ have lost enough energy to be completely suppressed by the discriminator. Besides, Møller scattering is kinematically forbidden at angles larger than 90° if the target electron is initially at rest.

The negligible influence of the effects discussed until now results partly from the fact that the solid angles in the present arrangement are smaller than in conventional Mott detectors, partly from the better energy resolution of 10 keV which is caused by the small active areas of the counters (25 mm^2). Before we discuss those spurious effects which need correction, we emphasize that additional potential errors arise by differences of the left and right detection channels of the analyzer, e.g., differences in detector efficiencies, in the solid angles subtended by the detectors and in electronics. This error source is eliminated by rotation of the counter system (including gold foil and diaphragms) through 180° to interchange the positions of the left and right detectors (collected intensities L,R and L',R', respectively). With $N^+=\sqrt{LL'}$ and $N^-=\sqrt{RR'}$ one obtains the measured asymmetry (cf. Ref. 1, Chap. 8.1.2c)

$$A_m=\frac{N^+-N^-}{N^++N^-}\ , \tag{5}$$

where the different counting-channel efficiencies are now eliminated.

This is, however, only warranted if differences in the dead-time corrections between the high- and low-intensity directions are taken into account, even though the two counting channels possess the same dead time τ. The relation between the measured counting rate n' and the corrected counting rate n is given by[16]

$$n=\frac{n'}{1-n'\tau}\ . \tag{6}$$

For the determination of τ, electrons were scattered at a gold foil and collected by two detectors, one of them situated at a large scattering angle (small intensities, dead-time corrections virtually negligible) and the other at a small angle. By changing the primary intensity, a change in the ratio of the collected intensities could be observed from which the dead time could be calculated. In our arrangement τ is 1.2×10^{-5} sec. A combination of Eq. (5) with Eq. (6) yields in first order a relation beween the

corrected asymmetry A_d and the uncorrected A_m:

$$A_d = A_m(1+\bar{n}\tau) , \tag{7}$$

where $\bar{n}$ is the average counting rate of the left and right detector. This equation offers the possibility to check the value of τ by asymmetry measurements which were performed on otherwise equal conditions with different primary intensities. All these measurements give the same result if a dead-time correction according to Eq. (7) with a dead time of 1.2×10^{-5} sec is made.

The asymmetry A_d has further to be corrected for scattering by the Pioloform backing. Assuming a zero Sherman function for low-Z Pioloform, van Klinken[4] derived for the corrected value

$$A = A_d\left[1+\frac{N_{P1}}{N_{Au1}}\right]\left[1+\frac{N_{P2}}{N_{Au2}}\right] , \tag{8}$$

where $N_{P1},N_{P2},N_{Au1},N_{Au2}$ are the (dead-time corrected) numbers of electrons scattered by Pioloform and gold in the first and second scattering, respectively. Mostly N_P/N_{Au} is less than 0.01 except for the thinnest foil (54 $\mu g/cm^2$) with scattering angles less than 90°. In this case the ratio (which has been directly observed by also bombarding a pure Pioloform foil of appropriate thickness) is sometimes 0.03, but the contribution to the final uncertainty in the corrected asymmetry remains negligible.

A correction considerably more complicated is required for the effects of both elastic and inelastic multiple and plural scattering. It was performed by extrapolation to zero foil thickness by a procedure that will be discussed in Sec. V.

Finally, we will briefly address a question which was raised by one of the referees and which has not really been discussed in the literature: Eq. (3) follows from the identity of polarizing and analyzing power ($S_p=S_a$) which holds in elastic scattering but, in general, not in inelastic scattering. Although, due to the limited energy resolution of 10 keV, our signal contains inelastically scattered electrons, there is not the least objection against exploiting Eq. (3) for the calibration of our polarimeter at 120°. Inelastically scattered electrons are usually deflected by small angles where no spindependent effects occur. They can reach large angles by subsequent elastic collisions which obey $S_a=S_p$. Consequently, these multiple processes do not invalidate this relationship. More dangerous could be single inelastic processes leading directly to the angle of observation. However, such events with energy losses ≤ 10 keV (our resolution) practically do not occur because their cross section is negligible. But even if they occured, they would not invalidate the aforementioned relationship. It has namely been shown for inelastic processes that polarizing and analyzing power "approach each other with increasing energy"[17] and that even in the range of a few hundred electron volts they differ not much from each other.[18] At the energies of the present experiment, which are larger by a factor of more than 100, any differences between these quantities would be far below what can be measured within our error limits.

D. Elimination of instrumental asymmetries

With the corrected asymmetries A_P and A_M of the polarization and monitor counters we were able to cope with instrumental asymmetries. First of all, the arrangement of the counters in the analyzer had to be checked for proper adjustment [correct distance ratio $h(45°)/h(120°)$]. This was done by asymmetry measurements, where large instrumental asymmetries were artificially introduced. As mentioned in the previous section, the trajectory of the polarized beam can be altered by a shift of the polarizer foil perpendicular to its own plane. The effect of this shift on A_P and A_M has been investigated experimentally and is presented for 50 keV in Fig. 9. It has been shown in Ref. 5 that for this kind of maladjustment the A_P versus A_M curve is linear with a slope q in a large region around $A_M=0$ and that q depends on the distance ratio $h(45°)/h(120°)$ of the monitor and polarization counters. Only for the correct counter arrangement discussed in Sec. IV A does the value of the slope q coincide with the value of $c=E(120°)/E(45°)$, which denotes the ratio of the relative change of the scattered intensities at 45° and 120°. In the 50-keV measurement we obtained agreement between the least-squares-fit result $q=0.188\pm0.003$ and the value of $c=0.189\pm0.003$. Similarly, in the 120-keV measurement we found $q=0.329\pm0.002$ and $c=0.333\pm0.006$.

Having ascertained the relation $q=c$ we could take advantage of the most important property of the correct arrangement: Only for $q=c$ is the relation between A_M and A_P independent of the origin of the misalignment of the polarized beam (cf. Ref. 5). If this is fulfilled one finds the genuine scattering asymmetry A_g from

$$A_g = A_P - c\,A_M , \tag{9}$$

as has been shown in Ref. 5, from which also follows that A_g is independent of the beam trajectory and of temporal variations in beam profiles and offers thus the possibility to check the stability of the measured values against beam variations (cf. the following section).

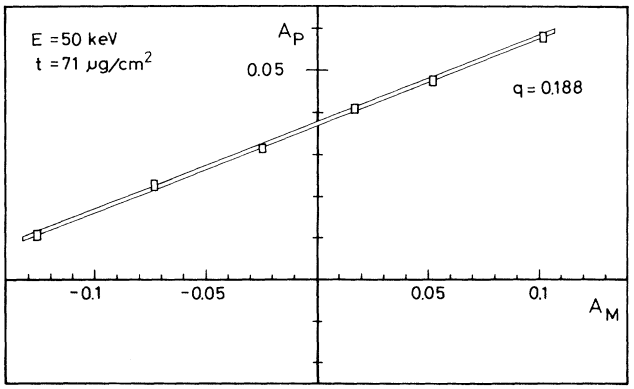

FIG. 9. Measured relationship between A_P and A_M, the asymmetries in the polarization counters and the monitor counters, resulting from misalignment of the polarized beam.

E. Analyzer calibration and measurement of S_{eff}

The calibration of the analyzer, i.e., the determination of its analyzing power S_a, was performed with two foils of equal thickness t in both scattering processes. For simplicity, the foil thickness parameter t and the subscript eff will be omitted in the following. The polarization of the single-scattered beam $[P(\theta)=S(\theta)]$ is according to Ref. 5

$$S(\theta)=\frac{A_P(\theta)-cA_M(\theta)}{S(120°)-cS(45°)}=\frac{A_g(\theta)}{S_a}\ , \tag{10}$$

where $S(120°)$ and $S(45°)$ are the Sherman functions at those angles where the counters are positioned and

$$S_a=S(120°)-cS(45°) \tag{11}$$

is the analyzing power S_a of the four-counter arrangement. Although $S(45°)$ is small, its value plays a role in a precision experiment and the determination of S_a requires two measurements. In the first measurement the analyzer was set at an angle of $\theta=120°$ and in the second one at $\theta=45°$. According to (10) and (11) the measured asymmetries are

$$\begin{aligned} A_g(120°)&=S(120°)[S(120°)-cS(45°)]\ , \\ A_g(45°)&=S(45°)[S(120°)-cS(45°)]\ . \end{aligned} \tag{12}$$

A combination of (12) with (10) yields the analyzing power

$$|S_a|=|A_g(120°)-cA_g(45°)|^{1/2}\ . \tag{13}$$

S_a depends only on measurable values and the small but finite and unknown value of $S(45°)$ is now eliminated.

After the analyzer had been calibrated, the measurements of the effective Sherman function S_{eff} as a function of θ, foil thickness t, and electron energy E could be performed according to

$$S_{\text{eff}}(\theta,t,E)=\frac{A_P(\theta,t,E)-cA_M(\theta,t,E)}{S_a(E)}\ , \tag{14}$$

which follows from (11). As described in Sec. II, t and θ were only varied in the scattering process number 1, while the analyzing power S_a relevant for the second scattering process remained unchanged during a measurement with fixed scattering energy.

In the 120-keV measurement, foils $\geq 87\ \mu g/cm^2$ were irradiated with 1 μA; for thinner foils the current was reduced to 0.5 μA to avoid damage of the foils. In the 50-keV measurement we needed only half the primary intensities to get comparable counting rates. The intensity ratio I_2/I_0 of the double scattered and primary electrons ranges between 1×10^{-9} and 1×10^{-11} which results in counting rates between 0.03 and 3 kHz for the polarization counters, whereas the rates of the monitor counters are larger by 50% (120 keV) and 100% (50 keV), respectively.

The smallest measurement cycle consists of counting times of 100 sec for each azimuthal position 0 and π of the rotatable analyzer. The number of cycles required for each measured value (between 40 and 800) is determined by the primary current and the thickness of the first scatterer. The parts of the foils that were hit by the beam were intentionally varied, so that for each measured value at least three different parts of a foil were irradiated. During a measurement the statistical uncertainty was continuously compared with the standard deviation (reproducibility) of the cycles. The agreement was excellent, apart from one case. This confirms the uniformity of the foils in structure and topology as well as the absence of fluctuations other than those caused by counting statistics, despite the fact that all the values were determined with high statistical accuracy ($\Delta S_{\text{eff}}\leq 2\times10^{-3}$). The exception is the 120-keV measurement at 45°, where the statistical uncertainty was reduced to 5×10^{-4} because of the small values of S_{eff}. In that case the standard deviation of the single measurements is 30% larger than the statistical uncertainty.[19] This was, however, not observed in the 50-keV measurement at 44°, where the statistical uncertainty was also reduced to 5×10^{-4}. We therefore conclude that in the 50-keV measurement the requirements for the correct arrangement of the monitor counters have been fulfilled a little bit better.

For the calibration of the analyzer at 120 keV we performed 260 measurement cycles at 120° which yield $A_g(120°)=0.07053(16)$. After 6 months, when all the asymmetry measurements were finished for one energy, we observed a thin layer of cracked hydrocarbon particles on the first scatterer due to intense radiation. To check the influence of this hydrocarbon cracking on the asymmetry results, we again determined $A_g(120°)$ by 80 further measurement cycles which yielded $A_g(120°)=0.070\,90(30)$. Because the two results coincide within the statistical uncertainty, we conclude that the hydrocarbon cracking on the first foil does not eliminate the symmetry of the two scatterers and thus does not invalidate Eq. (3). For the final determination of S_a, all results of the 360 measurement cycles of A_g were evaluated, where we again observed coincidence of the statistical uncertainty and the reproducibility. At 120 keV we obtained $S_a=0.2662\pm0.0006(0.2\%)$ and at 50 keV $S_a=0.2265\pm0.0007(0.3\%)$. The quoted uncertainties result from the counting statistics and from the uncertainty in the determination of the first scattering angle.

V. RESULTS

In this section we will discuss the results on the effective Sherman function S_{eff} that have been measured with the calibrated analyzer at scattering energies of 50 and 120 keV. Figures 10–12 present the dependence of S_{eff} on the thickness of the scattering foil for various angles above and below 90°. The reason for the difference in angle between the 50- and the 120-keV data has been explained in Sec. III. The results turned out to be highly reproducible owing to our method of eliminating instrumental asymmetries. The progress is demonstrated by Fig. 2, where our results are compared with those of van Klinken,[4] which are the most accurate absolute values until today. All the measured values including those not shown in the diagrams are listed in Tables II and III. The uncertainties given there result from counting statistics and the uncertainty of the calibration of the analyzer.

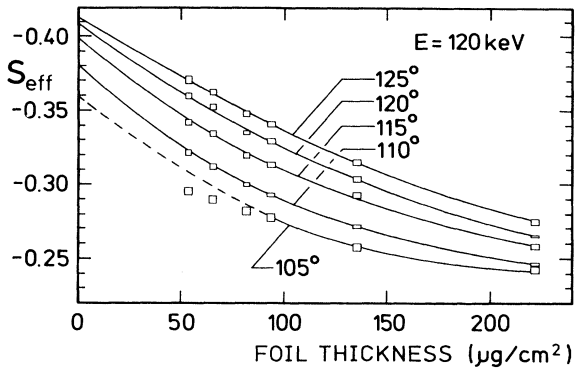

FIG. 10. Effective Sherman function for 120 keV at scattering angles $>90°$ vs foil thickness. The size of the rectangles represents the experimental uncertainties. The curves are explained in the text.

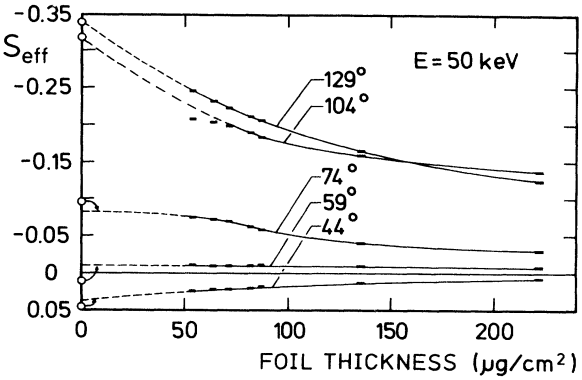

FIG. 12. Effective Sherman function for 50 keV. The curves are guides to the eye. The circles represent the theoretical results of Bühring (Ref. 6). The size of the rectangles represents the experimental uncertainties.

Figures 10 and 11 present most of our data at 120 keV. The experimental values of $S_{\text{eff}}(t)$ and the theoretical values of $S_{\text{eff}}(0)$ by Bühring[6] are fitted by curves that guide the eyes. This simple fit procedure was chosen because presently a better established method is not available. Although the experimental and theoretical data match very well, we would not like to claim a precise confirmation of the theoretical results; but there is certainly no contradiction to the theoretical data. A considerable improvement of Hnizdo's Monte Carlo calculation[20] would be an invaluable help for solving the problems of extrapolation to $t=0$ and comparison with theory especially for scattering angles smaller than 120°. Merely at 105° some data are not connected by our fit (broken line) which may be explained as follows: Electrons that are scattered by 105° after normal incidence leave the target under a grazing angle (15°), so that the values of S_{eff} are more and more affected by the surface roughness as the foil thickness decreases. A similar behavior at 75° was not observed, presumably because S_{eff} depends only slightly on foil thickness at this angle (see Fig. 11).

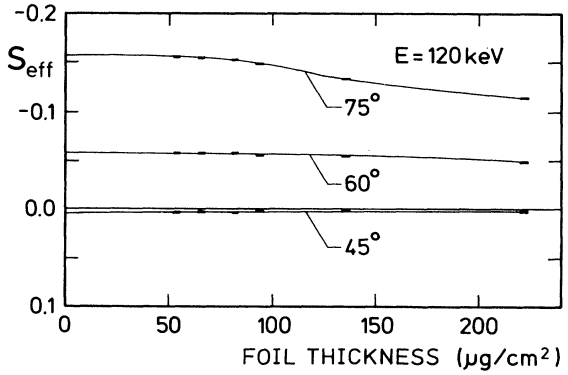

FIG. 11. Effective Sherman function for 120 keV at scattering angles $<90°$ vs foil thickness. The size of the rectangles represents the experimental uncertainties. The curves are explained in the text.

Figure 12 shows some of the data at 50 keV. The dependence of S_{eff} on foil thickness is stronger than that at 120 keV, which makes a comparison with theoretical results more difficult. Not only at 104° (to a smaller extent also at 109° and 114°) but also at 74° was it impossible to find a reasonable fit which describes not only the experimental data, but also the theoretical values for $t=0$. Again, we take this as an influence of the surface roughness of the foils. Furthermore, the results at 59° indicate a different sign of S_{eff} than does the theoretical calculation, which cannot be explained by shortcomings in the extrapolation procedure. Such a difference in sign has also been observed at 46.5 keV and 60° by van Klinken.[4]

Although there is no universal fit to our experimental results, it turned out that, for the largest angles studied, there exists a reliable method of extrapolating the data to zero foil thickness. This makes possible a comparison with the theoretical results calculated for single scattering through these angles. That is why in the following we will dwell upon the problem of extrapolation to $t=0$.

While extrapolation to foil thickness zero is a general procedure that is widely used, this procedure is not unique[2] because there exists no reliable theoretical or experimental guide on the dependence of S_{eff} on foil thickness t. The present precise double-scattering experiment cannot solve this problem either. First of all, the foils are not thin enough to substantiate an unequivocal relationship, and any attempt to reduce this uncertainty by using extremely thin gold foils is dangerous, as discussed in Sec. IV A. Secondly, our results indicate that the shape of the extrapolation curve changes with scattering angle, which aggravates the solution of this problem.

The foil-thickness extrapolation has first been treated theoretically by Wegener.[21] He expanded the scattering power $N(\theta,\pm\pi/2)$ for normal incidence of transversely polarized electrons in terms of t up to the second order

$$N(\theta,\pm\pi/2)\sim t\{(1+\beta t)[1\pm PS(\theta)]\mp\alpha t PS(\theta)\}\ , \qquad (15)$$

where α and β, which depend on energy, scattering angle,

TABLE II. Results of the 120-keV measurement. The signs result from comparison with theoretical data.

t (μg/cm^2)	S_{eff}(130°)	S_{eff}(125°)	S_{eff}(120°)
222.0(2.0)	−0.2821(20)	−0.2745(17)	−0.2653(8)
135.4(1.9)	−0.3203(19)	−0.3151(18)	−0.3033(18)
94.0(1.8)	−0.3444(18)	−0.3406(17)	−0.3289(16)
82.1(1.4)	−0.3489(19)	−0.3474(17)	−0.3344(15)
65.7(1.5)	−0.3633(22)	−0.3623(22)	−0.3519(18)
54.0(1.3)	−0.3674(24)	−0.3702(23)	−0.3594(22)
t (μg/cm^2)	S_{eff}(115°)	S_{eff}(110°)	S_{eff}(105°)
222.0(2.0)	−0.2583(16)	−0.2459(12)	−0.2430(10)
135.4(1.9)	−0.2927(18)	−0.2715(15)	−0.2574(10)
94.0(1.8)	−0.3129(17)	−0.2923(10)	−0.2772(11)
82.1(1.4)	−0.3196(17)	−0.2993(14)	−0.2821(12)
65.7(1.5)	−0.3341(17)	−0.3118(18)	−0.2896(13)
54.0(1.3)	−0.3416(21)	−0.3215(18)	−0.2949(13)
t (μg/cm^2)	S_{eff}(75°)	S_{eff}(60°)	S_{eff}(45°)
222.0(2.0)	−0.1143(7)	−0.0489(5)	+0.0026(2)
135.4(1.9)	−0.1332(6)	−0.0549(4)	+0.0012(3)
94.0(1.8)	−0.1487(7)	−0.0559(7)	+0.0020(3)
82.1(1.4)	−0.1520(7)	−0.0572(5)	+0.0037(5)
65.7(1.5)	−0.1541(8)	−0.0572(8)	+0.0030(5)
54.0(1.3)	−0.1555(9)	−0.0575(9)	+0.0035(9)

TABLE III. Results of the 50-keV measurement.

t (μg/cm^2)	S_{eff}(129°)	S_{eff}(124°)	S_{eff}(119°)
222.0(2.0)	−0.1242(10)	−0.1263(9)	−0.1293(8)
135.4(1.9)	−0.1659(11)	−0.1649(10)	−0.1633(9)
87.4(1.5)	−0.2055(13)	−0.2043(11)	−0.2014(11)
82.1(1.4)	−0.2107(12)	−0.2096(10)	−0.2072(14)
71.6(1.5)	−0.2227(15)	−0.2239(14)	−0.2216(11)
64.1(1.6)	−0.2320(16)	−0.2303(15)	−0.2286(13)
54.0(1.3)	−0.2450(15)	−0.2446(16)	−0.2406(14)
t (μg/cm^2)	S_{eff}(114°)	S_{eff}(109°)	S_{eff}(104°)
222.0(2.0)	−0.1301(9)	−0.1329(9)	−0.1371(10)
135.4(1.9)	−0.1584(10)	−0.1591(10)	−0.1589(11)
87.4(1.5)	−0.1969(12)	−0.1903(8)	−0.1836(12)
82.1(1.4)	−0.1986(10)	−0.1915(12)	−0.1893(12)
71.6(1.5)	−0.2089(14)	−0.2046(13)	−0.1986(11)
64.1(1.6)	−0.2167(11)	−0.2083(13)	−0.2030(11)
54.0(1.3)	−0.2251(14)	−0.2154(12)	−0.2073(14)
t (μg/cm^2)	S_{eff}(74°)	S_{eff}(59°)	S_{eff}(44°)
222.0(2.0)	−0.0302(6)	−0.0083(5)	+0.0067(6)
135.4(1.9)	−0.0406(8)	−0.0095(6)	+0.0127(6)
87.4(1.5)	−0.0587(8)	−0.0106(5)	+0.0181(5)
82.1(1.4)	−0.0619(8)	−0.0103(4)	+0.0207(6)
71.6(1.5)	−0.0694(9)	−0.0103(6)	+0.0214(3)
64.1(1.6)	−0.0728(10)	−0.0105(7)	+0.0223(5)
54.0(1.3)	−0.0745(9)	−0.0115(6)	+0.0242(6)

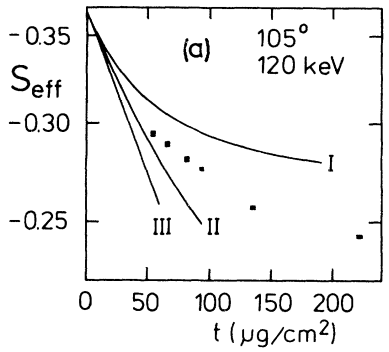

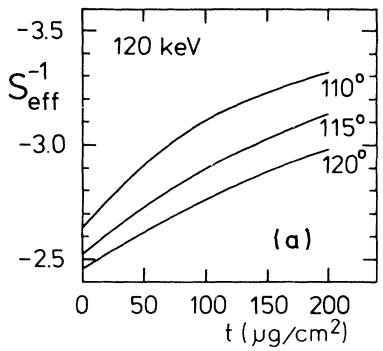

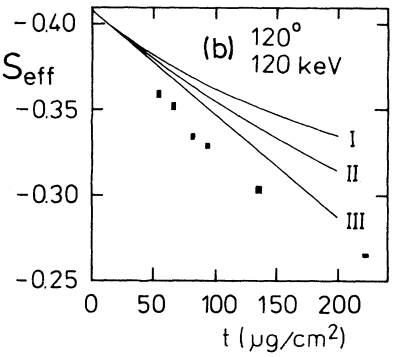

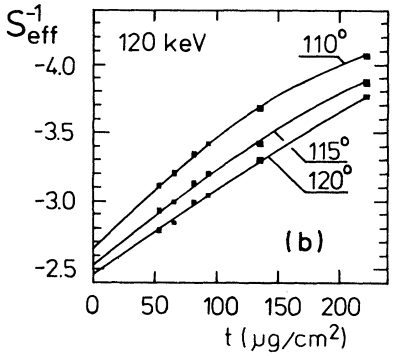

FIG. 13. Effective Sherman function vs foil thickness. Solid lines calculated from Eqs. (16), (18), and (17) (curves I, II, and III, respectively) using the coefficients α and β from Wegener's (Ref. 21) tables. Rectangles: experimental results. The size of the rectangles represents the experimental uncertainties.

FIG. 14. Effective Sherman function vs foil thickness. (a), calculated from Eq. (16); (b), results of this experiment. At foil thickness zero the values calculated by Bühring (Ref. 6) have been used. The lines in (b) guide the eyes and illustrate how the curvature decreases as the angle increases.

and slightly on foil thickness t, can be calculated from tabulated values given in Ref. 21. Using Eqs. (1) and (15), the t-dependent asymmetry function can be written

$$S_{\text{eff}}(t)=S(0)\left[1-\frac{\alpha t}{1+\beta t}\right], \tag{16}$$

where $S(0)=S_{\text{eff}}(t=0)$. Wegener suggested the following approximation, which holds when αt and βt are small compared to unity:

$$S_{\text{eff}}(t)\approx S(0)(1-\alpha t)\ . \tag{17}$$

Other possible approximations are

TABLE IV. $S(t=0,120\text{ keV})$. Results of a weighted linear least-squares fit of S_{eff}^{-1} vs t (including the error of the relative foil thicknesses and of S_{eff}) compared with different theoretical values. The fits and the accompanying reduced χ^2 values were calculated according to Ref. 25. At 120° the values of the 222-μg/cm^2 foil was not used in the extrapolation procedure because it clearly deviates from the straight line (cf. Fig. 14), on which our extrapolation is based.

θ	Extrapolation	χ_ν^2	Bühring[a]	Lin[b]	Holzwarth and Meister[c]	Ross and Fink[d]
120°	−0.4099(44)	1.63	−0.4068	−0.4072	−0.400	−0.404
125°	−0.4158(28)	0.47	−0.4108		−0.401	
130°	−0.4091(29)	0.59	−0.4074	−0.4067	−0.394	

[a]Reference 6.
[b]Reference 22.
[c]Reference 23.
[d]Reference 24.

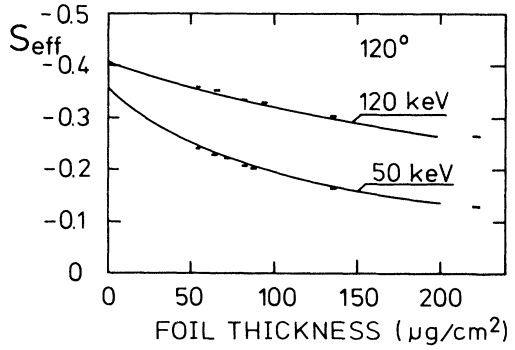

FIG. 15. Decrease of S_{eff} with foil thickness according to the Monte Carlo calculation of Hnizdo (Ref. 20) (solid lines) compared to our data points. At $t=0$ the values calculated by Bühring (Ref. 6) have been used.

$$\frac{1}{S_{\text{eff}}(t)} \approx \frac{1}{S(0)}(1+\alpha t) \tag{18}$$

and

$$S_{\text{eff}}(t) \approx S(0)e^{-\alpha t} . \tag{19}$$

Except for Eq. (16), all of these approaches have been used by experimentalists as a theoretical basis for extrapolation (cf. Ref. 2 and references therein). In order to see the influence of the approximations, we calculated $S_{\text{eff}}(t)$ according to Eqs. (16), (17), and (18), where we used the coefficients α and β from Wegener's tables and took for $S(0)$ the theoretical values of Bühring.[6] Figure 13 illustrates that the approaches (16)–(18) together with the values of α and β from Wegner's tables are not adequate for the foils that have been used in this experiment.

Although Eq. (16) does not properly describe the decrease of S_{eff} with increasing foil thickness, it is the only one which reflects the fact that the shape of the extrapolation curve changes with scattering angle. This is shown in Fig. 14 where, for different scattering angles, S_{eff}^{-1} has been plotted versus t because this plot eliminates much of the curvature of the extrapolation curve. Both experimental and theoretical data indicate that in a S_{eff}^{-1} versus t plot one obtains a decrease of the curvature as the angle increases and a transition into straight lines for $\theta \geq 120°$, a result that is also borne out by our data for 125° and 130° at 120 keV (not shown in Fig. 14) and at 50 keV for angles larger than 119°. Figure 15 shows that the Monte Carlo calculations of Hnizdo,[20] which are also very well approximated by a straight line in an S_{eff}^{-1} versus t plot, are in remarkable agreement with our data at 120°.

On the basis of these results it seems most appropriate to use an S_{eff}^{-1} versus t plot for extrapolation to foil thickness zero in order to compare with theoretical results at large angles. Tables IV and V show the results of a linear least-squares fit[25] in such a plot, where the data have been weighted with the error of the relative foil thickness and S_{eff}. At 120 keV, two of the extrapolated values of Table IV agree with the calculated data of Bühring[6] and Lin.[22] Only the 125° values is somewhat too high. In contrast, our data disagree with the theoretical calculations of Holzwarth and Meister.[23] It is interesting to note that similar conclusions—agreement with results of Bühring[6] and of Lin,[22] disagreement with Holzwarth and Meister[23]—followed from former cross-section measurements for electron scattering by free mercury atoms.[26] At 50 keV and 119° all the calculated values agree with the experimental result, whereas at larger angles our values are above the theoretical data. Still, the values of Bühring[6] and Lin[22] are the closest to our experimental data. Assuming an uncertainty of 3% for the procedure of extrapolation as quoted by Fletcher *et al.*,[2] we find agreement with calculations of Bühring and of Lin at least for the scattering angles and energies given in Tables IV and V.

ACKNOWLEDGMENTS

We are grateful for the cooperation of the late Dr. K. Jost, whose help in this project was extremely valuable. This work was supported by the Sonderforschungsbereich 216 of the Deutsche Forschungsgemeinschaft.

TABLE V. Same as Table IV for $S(t=0, 50\text{ keV})$ and for $t \leq 135\ \mu\text{g/cm}^2$. The theoretical values of Lin and of Ross and Fink hold for 120°, 125° and 130°, whereas the values of Holzwarth and Meister are interpolated from data for 46, 63, and 100 keV.

θ	Extrapolation	χ_ν^2	Bühring[a]	Lin[b]	Holzwarth and Meister[c]	Ross and Fink[d]
119°	−0.356(6)	0.85	−0.356	−0.356	−0.351	−0.352
124°	−0.362(7)	0.43	−0.353		−0.346	
129°	−0.360(6)	0.04	−0.343	−0.341	−0.334	

[a]Reference 6.
[b]Reference 22.
[c]Reference 23.
[d]Reference 24.

[1]J. Kessler, *Polarized Electrons,* 2nd ed. (Springer-Verlag, Berlin, 1985).
[2]G. D. Fletcher, T. J. Gay, and M. S. Lubell, Phys. Rev. A **34**, 911 (1986).
[3]J. Kessler, Rev. Mod. Phys. **41**, 3 (1969).
[4]J. van Klinken, Nucl. Phys. **75**, 161 (1966); Ph.D. thesis, University of Groningen, 1965.
[5]A. Gellrich and J. Kessler, Rev. Sci. Instrum. **61** (1990).
[6]W. Bühring, private communication. These computations are of essentially the same type as those described earlier [W. Bühring, Z. Phys. **212**, 61 (1968)], for a screened (Au) Coulomb potential consisting of three Yukawa terms with screening parameters according to Eqs. (38) and (39) of W. Bühring, Z. Phys. A **317**, 241 (1984).
[7]A. R. Brosi, A. I. Galonsky, B. H. Ketelle, and H. B. Willard, Nucl. Phys. **33**, 353 (1962).
[8]W. Raith, in *Atomic Physics,* edited by B. Bederson, V. W. Cohen, and F. M. J. Pichanick (Plenum, New York, 1969), p. 389.
[9]U. Heinzmann, J. Phys. B **11**, 399 (1978).
[10]V. Eckardt, A. Ladage, and U. V. Moellendorff, Phys. Lett. **13**, 53 (1964).
[11]R. Gauder, E. Speller, U. Zierer, O. Boslau, A. Hilscher, and K.-W. Hoffmann, Z. Phys. A **330**, 423 (1988).
[12]K. Jost, in *Proceedings of the International Symposium on Correlation and Polarization in Electronic and Atomic Collisions,* edited by Paul A. Neill, Kurt H. Becker, and Michael H. Kelley, NIST Special Publication 789 (NIST, Gaithersburg, MD, 1990), p. 76.
[13]D. M. Lazarus and J. S. Greenberg, Phys. Rev. D **2**, 45 (1970).
[14]L. Reimer and K. Freking, Z. Phys. **184**, 119 (1965).
[15]L. L. Kazmerski and D. M. Racine, J. Appl. Phys. **46**, 791 (1975).
[16]J. W. Müller, Nucl. Instrum. Methods **112**, 47 (1973).
[17]K. Bartschat and K. Blum, J. Phys. B **15**, 2747 (1982).
[18]W. Eitel and J. Kessler, Z. Phys. **241**, 355 (1971).
[19]A. Gellrich, Ph.D. thesis, University of Münster, 1989.
[20]V. Hnizdo, Nucl. Instrum. Methods **109**, 503 (1973).
[21]H. Wegener, Z. Phys. **151**, 252 (1958); see also J. S. Greenberg, D. P. Malone, R. L. Gluckstern, and V. W. Hughes, Phys. Rev. **120**, 1393 (1960).
[22]S. R. Lin, Phys. Rev. A **133**, 965 (1964).
[23]G. Holzwarth and H. J. Meister, Nucl. Phys. **59**, 56 (1964); *Tables of Asymmetry, Cross Sections and Related Functions for Mott Scattering of Electrons by Screened Au and Hg Nuclei* (University of Munich, Munich, 1964).
[24]A. W. Ross and M. Fink, Phys. Rev. A **38**, 6055 (1988).
[25]Philip R. Bevington, *Data Reduction and Error Analysis for the Physical Sciences* (McGraw-Hill, New York, 1969).
[26]J. Kessler and N. Weichert, Z. Phys. **212**, 48 (1968).